Thermally induced structural transitions in epoxy thermoset polymer networks and their spectroscopic responses

Derek Dwyer, Sara Isbill, Zachary Brubaker, Jong K. Keum, Wim Bras, Jennifer L. Niedziela*

Oak Ridge National Laboratory, PO Box 2008 MS-6117, Oak Ridge, Tennessee, 37831

KEYWORDS: wide-angle x-ray scattering, epoxy thermoset, principal component analysis, polymer, Bisphenol A epoxy resin

ABSTRACT

The polymer network structure of epoxy thermosets plays a significant role in its final material properties. However, the effects of mild thermal exposure on these network structures are poorly studied. In this work, wide angle x-ray scattering was used to investigate the polymer network structure of two epoxy thermosets: homopolymerized bisphenol A (BPA) epoxy resin and BPA epoxy resin cured with a polyether amine hardener (BPA/T-403). Using density functional theory and wide-angle x-ray scattering, insights into the polymer network structure were obtained. Diffraction features were determined to originate from hardener-to-hardener molecular distance, perpendicular π–π stacking of aromatic p-phenylene rings, and the average Carbon–Carbon

distance in the polymer. Thermal exposure was found to permanently alter these structural features for both thermosets, with an increase in π–π stacking distance. Homopolymerized BPA had an additional decrease in the hardener-to-hardener distance. These structural alterations were found to be detectable using Fourier transform infrared spectroscopy and Raman spectroscopy, with changes in the hardener-to-hardener distance having the largest variations in the resulting spectra specifically at the aromatic and ether frequencies.

INTRODUCTION

Since their invention, epoxy thermosets have demonstrated a broad range of utility, from protective surface coatings to composites used in structural applications, thanks to their diverse range of material properties.[1] These properties can be controlled by manipulating the thermosets' curing conditions, hardener type, and epoxy-to-hardener ratio.[2-7] Other less controllable factors that have been shown to affect the thermosets' material properties are polymer network structures such as polymer packing,[8, 9] which is intrinsic to all thermosetting materials, and crystalline defects.[10] An example of the effect that polymer packing can have on thermoset material properties is shown by altering the isomer content of bisphenol F–based epoxy thermosets.[8] Thermosets prepared with high concentrations of ortho-ortho bisphenol F isomers experience weakening of the polymer network and lower chemical resistance compared with thermosets using para or ortho-para isomers. These differences in material properties were directly related to the packing of the polymer network. Therefore, a better understanding of these intrinsic polymer network structures and the effect that thermal exposure has on these structures would improve understanding of the resulting thermoset properties and provide routes of improvement for thermosets used at elevated temperatures.

X-ray diffraction–based techniques are powerful tools for the direct elucidation of material structures. Wide-angle x-ray scattering (WAXS), in particular, is used routinely for investigating polymers.[11-16] A number of studies have used WAXS for investigating the structural transformation of liquid crystal polymers integrated in polymer thermosets.[17-20] However, limited work uses WAXS to study the structural transitions of the epoxy polymer networks, which are generally considered amorphous.[21-23] Even though WAXS is most powerful when studying crystalline materials, structural information is also contained in the WAXS pattern of amorphous—and even liquid—materials.[24] Understanding the WAXS pattern and the corresponding structural features of the amorphous epoxy thermoset could illuminate a subtle change in the polymer network from thermal perturbations, which may affect material performance. In this work, WAXS was used to investigate the polymer network structures of two different epoxy thermoset formulations. Density functional theory calculations were performed to identify the corresponding network features observed in the WAXS patterns. Finally, Fourier transform infrared spectroscopy (FTIR) and Raman spectroscopy coupled with principal component analysis (PCA) were used to determine if changes observed in the polymer network could be detected spectroscopically.

METHODS

MATERIALS

Epon 828 (bisphenol A [BPA] epoxy resin, M.W. = 384 g/mol) and Epikure 3253 (M.W. = 265 g/mol) were purchased from Miller-Stephenson. Trimethylolpropane tris[poly(propylene glycol), amine terminated] ether (T-403, M.n. = 440 g/mol) hardener was purchased from Millipore Sigma. All materials were used as received. The goals for selecting these formulations were to observe features that would be most broadly applicable to other epoxy-based thermosets. Selection of BPA epoxy resin was chosen because is it one of the most used epoxy resins for thermosets. T-403 was

chosen as a representation for a common class of hardeners, chain aliphatic polyamines. The Epikure catalyst was chosen for its stark contrast to common epoxy-amine reactive chemistry resulting in self polymerized epoxy networks with reduced alcohol functional group content.

EPOXY THERMOSET SYNTHESIS

Homopolymerized BPA (BPA-H) thermoset was synthesized by preheating 1.150 g of BPA resin (Epon 828) at 85 °C for 1 h. Epikure 3253 (75 μL) was added and mixed by hand. The Epikure 3253 catalysts initiates homopolymerization between epoxide groups without hardener. As a result, the chemical functionality of the polymer network is distinctly different from amine hardener-based thermosets with no amine functional groups and a reduced alcohol functional group content. While higher concentrations of catalyst will induce faster curing kinetics the amount chosen in this work were arbitrary and were selected based on the lower bounds of the volumetric tool used. The BPA/T-403 amine hardener-based thermoset was synthesized by preheating 1.152 g of BPA resin at 85 °C for 1 h. T-403 (449 μL) was added and mixed by hand to make a 2:1 ratio of epoxide groups to primary amine functional groups. Both samples were degassed at 85 °C and put into a glass capillary with a diameter of 2 mm, where they were cured overnight at 85 °C.

WAXS MEASURMENTS

WAXS measurements were performed on a Xenocs Xeuss 3.0 instrument equipped with D2+ MetalJet x-ray source (Ga Kα, 9.2 keV, λ = 1.341 Å). The capillaries filled with sample were aligned perpendicular to the direction of the incident x-ray beam (transmission mode), and the scattering beam was recorded on a Dectris Eiger 2R 4M hybrid photon counting detector with a pixel dimension of 75 × 75 μm^2, where the x-ray exposure time for each measurement was 20 s. The collected 2D isotropic WAXS images were circularly averaged and expressed as absolute

intensity versus Q, where $Q = (4\pi\sin\theta)/\lambda$ after transmission correction and subtraction of background scattering. To calibrate the measured intensities to absolute scale intensities, the direct beam intensity was used. The Q range investigated in this work was 0–3.5 $Å^{-1}$. The d-spacing was calculated using the relation $Q = 2\pi/d$. A differential scanning calorimetry (DSC) stage from Linkam[25] was used for in situ heating (i.e., online curing) measurements. Prepolymer sample was prepared in an aluminum DSC pan with a lid. The sample was loaded into the DSC stage and heated to 85 °C while measurements were taken.

COMPUTATION

A large molecular representation of a portion of the BPA-H thermoset network was created based on the known alcohol epoxy reaction for homopolymerized thermosets and the resulting connectivity from the reaction. The starting structure was created by converting the 2D SMILES notation of the representative molecule to three-dimensional space using the Avogadro visualization software. The molecular representation of the thermoset was relaxed using the NWChem 6.8 electronic structure theory software.[26] The M06-2X exchange correlation functional[27] with Grimme's D3 dispersion corrections[28] was combined with the cc-pVDZ basis set of Dunning[29-33] to find the minimum energy geometry. The structure was composed of seven BPA monomers, resulting in 301 atoms. All atoms were relaxed until the maximum and root mean square of the coordinates were less than 0.0045 Å and 0.003 Å, respectively, and the maximum and root mean square of the Cartesian step were less than 0.018 Å and 0.012 Å, respectively.

SPECTROSCOPIC MEASURMENTS

FTIR measurements were taken on a Bruker INVENIO R FTIR with an attenuated total reflectance attachment. Measurements were taken with a scan range of 4500–350 cm^{-1} at a resolution of 3 cm^{-1}. Raman spectra were collected on a Renishaw Invia Raman microscope using

a 785 nm excitation wavelength and grating with 1200 lines/mm, yielding a resolution of 2 cm^{-1}. For all measurements, the laser power was held below 500 μW. Principal Component Analysis (PCA) was performed on the resulting FTIR and Raman spectra using Origin Pro 2022 software with Principal Component Analysis for Spectroscopy v1.30. Calculation of curing extent was determined using equation 1.[34]

$$\alpha = 1 - \left({}^{A_{914}}\!/_{A_{1607}}\right)_t / \left({}^{A_{914}}\!/_{A_{1607}}\right)_0 \quad (1)$$

Where α is the reaction extent, A_{914} and A_{1607} at *t* are the absorbance of the epoxide ring and stable aromatic peak respectively at some time after cure onset. A_{914} and A_{1607} at *0* are the absorbance of the epoxide ring and stable aromatic peak respectively before curing commences.

RESULTS AND DISCUSSION

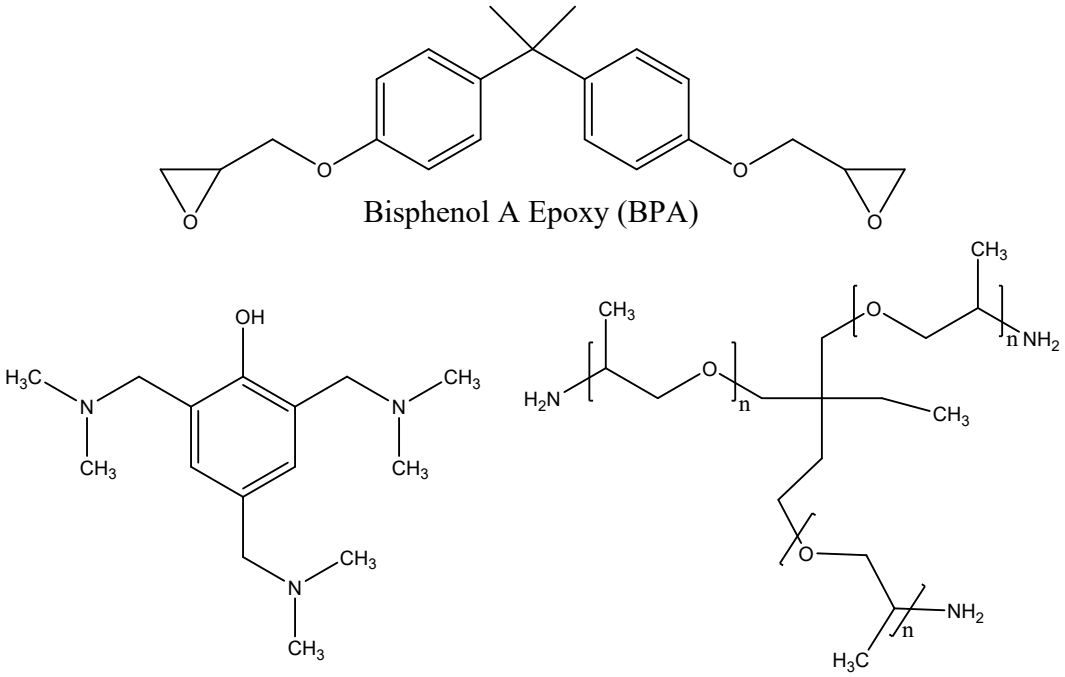

Figure 1. Ideal chemical structures of BPA epoxy resin, T-403 hardener, and Epikure 3253 catalyst.

The chemical structures of the prepolymer components are shown in **Figure 1**. While the T-403 hardener is integrated into the polymer network the Epikure 3253 catalyst is not. WAXS patterns of the BPA resin and the thermosets BPA-H and BPA/T-403 are shown in **Figure 2**. BPA epoxy resin has two visible peaks in WAXS at 1.95 $Å^{-1}$ (π–π) and 3.73 $Å^{-1}$ (C–C), which correspond to *d*-spacings of 3.22 and 1.68 Å, respectively. Curing results in a significant increase of the π–π distance from 3.22 Å to larger distances of 3.60 Å and 3.64 Å for BPA-H and BPA/T-403, respectively. A third peak (H–H) also emerges at the larger *d*-spacing of 12.69 Å for BPA-H and 9.79 Å for BPA/T-403. For π–π, *d*-spacing resembles aromatic π–π stacking resulting from the high concentration of aromatic groups in the epoxy resin.[35] Distances associated with C–C are the average carbon-carbon distances in the material. Finally, the new structure (H–H) has been attributed previously to either the ordering of the bisphenol epoxy monomers or the ordering of hardeners from curing.[22, 23]

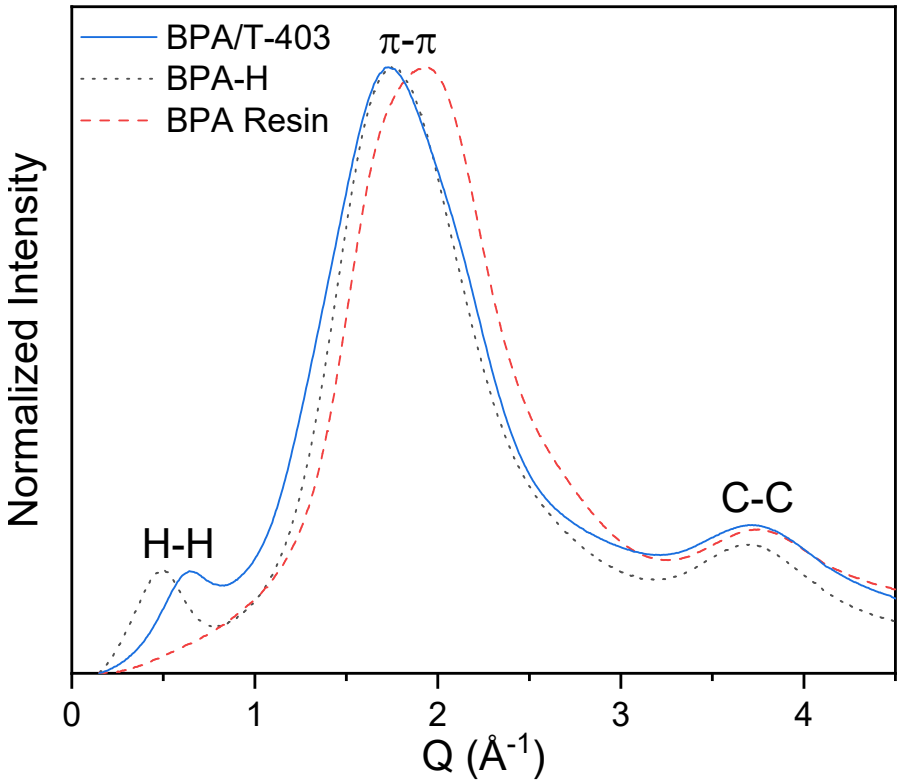

Figure 2. WAXS patterns of BPA-H and BPA/T-403 thermosets and BPA prepolymer epoxy resin. Two structural features were observed for the uncured BPA epoxy (π–π and C–C), and a third structural feature manifested after curing (H–H).

Curing was performed online during WAXS acquisition to validate that H–H was a result of the curing process and not from some other structural feature in the prepolymer formation. At room temperature before significant curing occurred, the uncured BPA-H formulation resembled the pure BPA resin (see **Figure 3**). Once the sample was heated to 85 °C, the new H–H structure emerged from the lower *Q*. The new structure decreased in distance up until 20 min of heating, after which time the structure remained constant. The growth of this peak as the curing proceeded supports the theory that H–H is a product of new structure formed from curing in the polymer network.

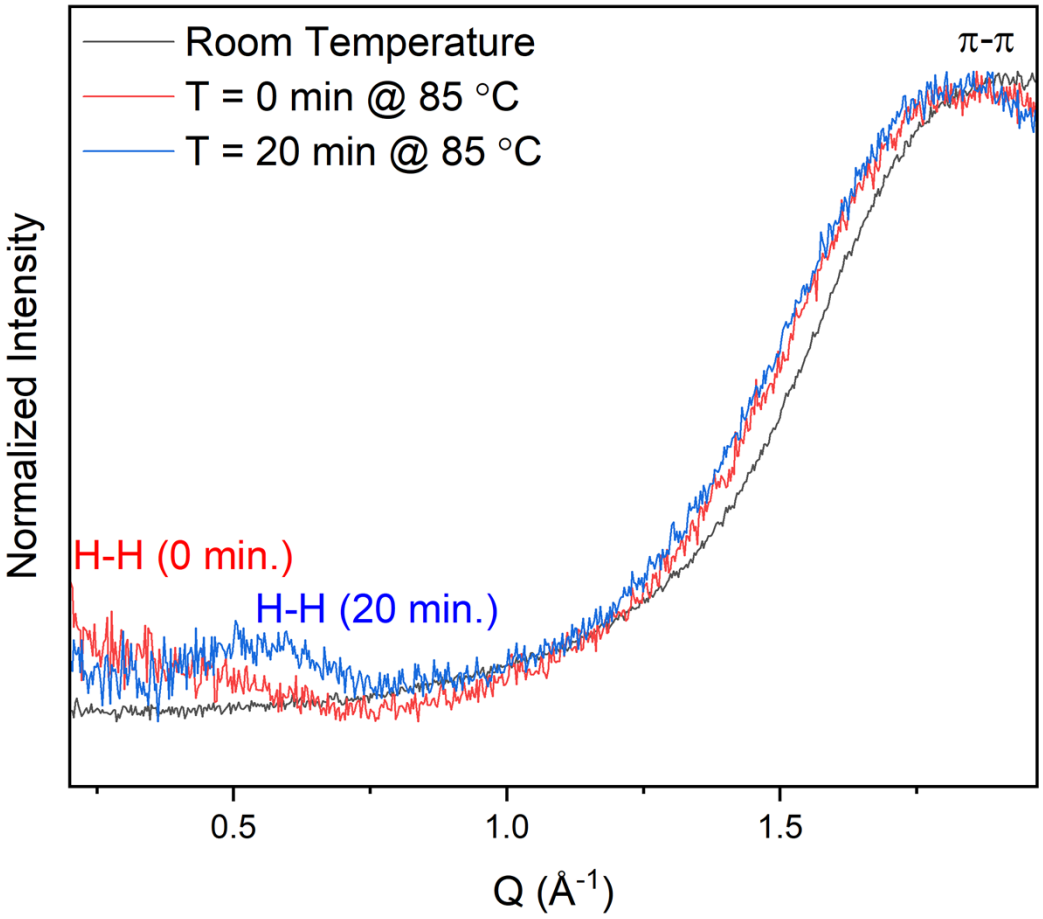

Figure 3. In situ WAXS patterns of BPA-H thermoset curing at 85 °C showing new structure formation (H–H) from curing. The H–H structure starts at larger distances but decreases as the curing proceeded until 20 min.

Density functional theory calculations were performed to support preliminary assignments of the structural edifices giving rise to H–H and π–π distances. These calculations were achieved using a molecular representation of the BPA-H thermoset, which is shown in **Figure 4A**. Results show evidence of π–π stacking at a distance of 3.7 Å (**Figure 4B**) and a hardener-to-hardener distance of 12.7 Å (**Figure 4C**). These results support the preliminary assignment of π–π and suggest that H–H is likely the distance between hardener regions in the polymer network rather than the ordering of the bisphenol epoxy monomers. The organization of the hardeners rather than

the epoxy monomers is conceptually sensible. The aromatic functional groups in the epoxy monomer make the structure more rigid than the hardener regions. This would make it easier for the epoxy monomers to hold the hardener groups out at fixed distances rather than vice versa, creating the observed structural features.

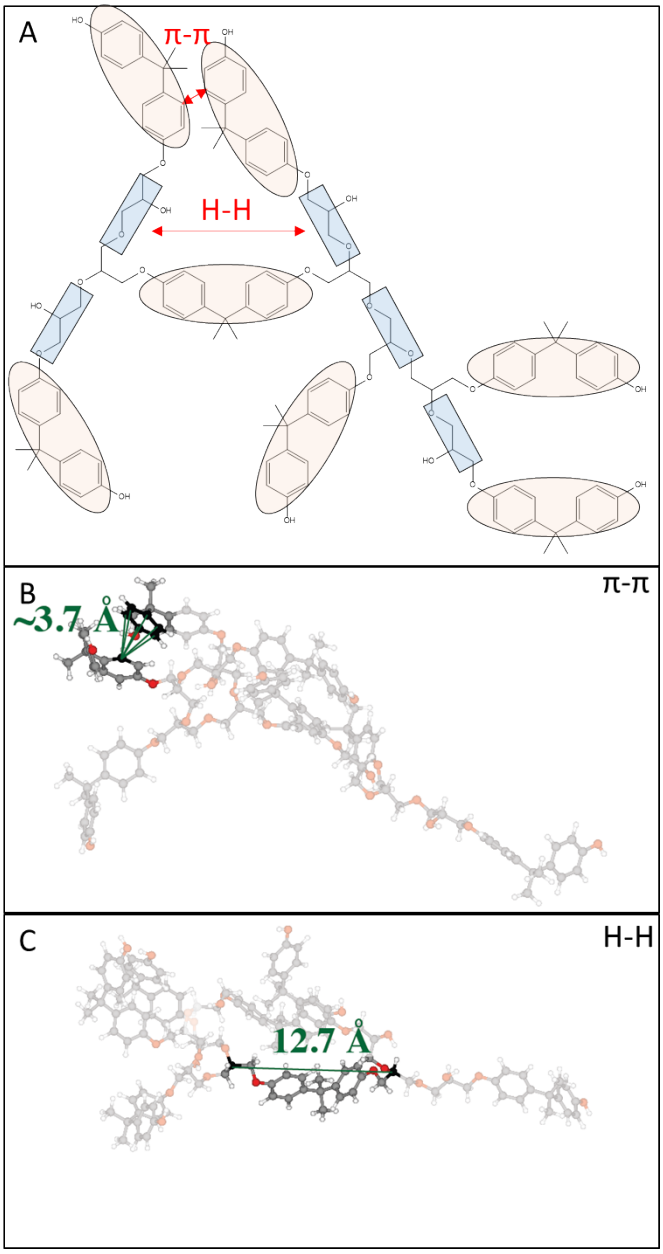

Figure 4. (A) Molecular representation of BPA-H polymer thermoset used in the computational model, and predicted sources of experimentally determined distances for structural features giving

rise to diffraction peaks (B) π–π and (C) H–H. π–π is confirmed to be from π–π stacking, and the computational model supports H–H originating from the hardener-to-hardener distance.

Thermosets were exposed to 150 °C for 1 h, which has been shown in previous work to be below the thermal degradation temperature.[36, 37] Therefore, any changes observed in the polymer network are associated with structural transitions and not thermal degradation. Thermal exposure at 150 °C was found to cause permanent alterations in the polymer networks of both thermosets (see **Figure 5**). Heating BPA-H caused the distances between hardeners to decrease by 1.89 Å. The relative intensity of this peak also decreased, indicating some loss of the structure. At the same time, the π–π stacking distance increased, which is visible by the shift of this peak to lower *Q* in the WAXS spectra. The H–H of the BPA/T-403 thermoset did not show any shifts in position after thermal exposure but did show a slight increase in relative intensity, indicating the formation of an additional H–H structure. Similar to BPA-H, the π–π stacking distance increased in BPA/T-403 after thermal treatment. A minor shift to lower *Q* (larger distances) for the C–C structure is also apparent in the BPA/T-403, but not in BPA-H. Therefore, thermal exposure of BPA/T-403 causes an increase in the π–π stacking distances and no change in the hardener-to-hardener distances.

The disconnected response between H–H and π–π supports the proposed premise that H–H is associated with the hardener-to-hardener distance. If H–H was associated with the distance between bisphenol groups, then as the *d*-spacing of π–π increased, the *d*-spacing of H–H should have increased as well, but this did not occur. Alternatively, if H–H was associated with the hardener-to-hardener distance, a difference in response between H–H and π–π for both thermosets could be explained because the two distances were no longer directly related to each other.

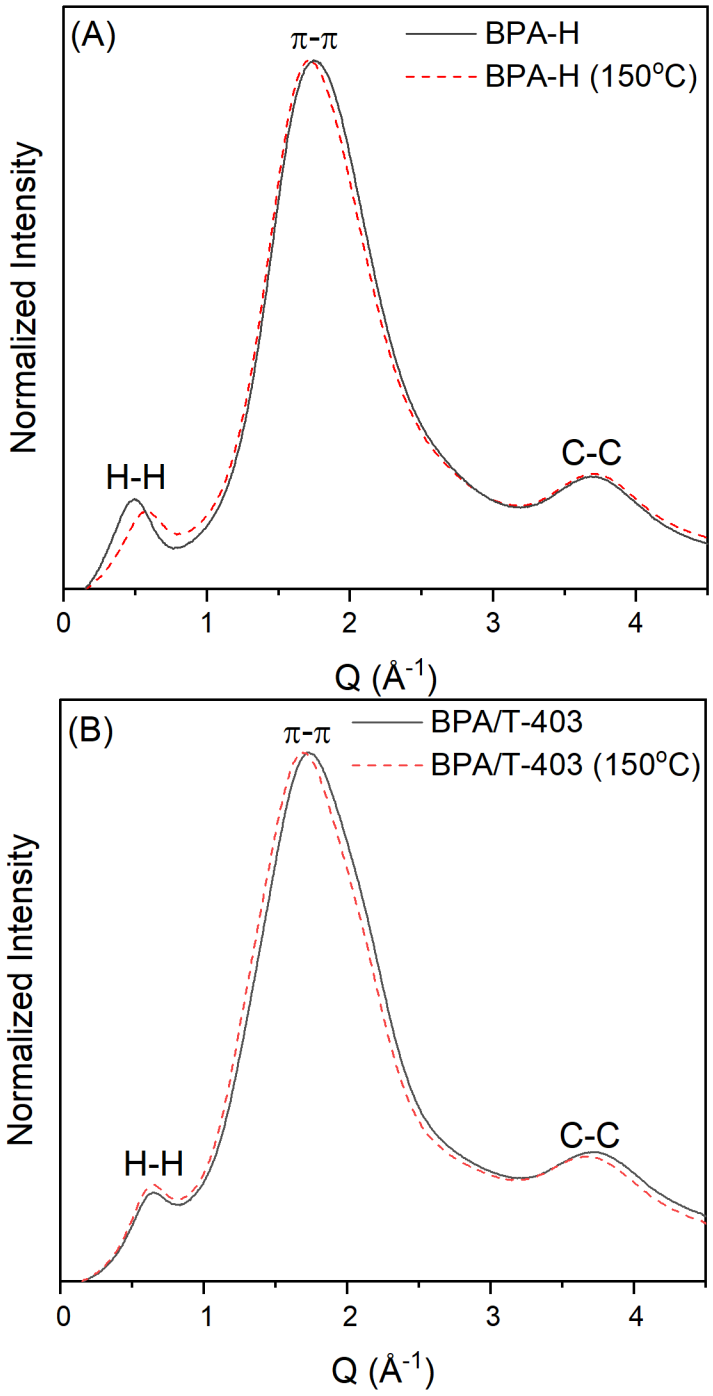

Figure 5. WAXS of (A) BPA-H and (B) BPA/T-403 thermosets before and after thermal treatment at 150 °C for 1 h. An increase in π–π stacking distance was observed for both thermosets, but BPA-H experienced a decrease in hardener-to-hardener distance.

FTIR and Raman spectroscopy were acquired to determine if the structural alterations observed in WAXS affected the molecular vibrational signature of the polymers. The FTIR and Raman spectra for BPA-H and BPA/T-403 thermosets are shown in **Figure 6**. The FTIR spectra of both thermosets share many common vibrational peaks associated with key functional groups in both thermosets, including ether peaks (1000–1300 cm^{-1}), aromatic stretches (1400–1700 cm^{-1}), and C–H alkane stretches (2850–3000 cm^{-1}). One of the most notable differences was the strong signal from the alcohol functional groups in BPA/T-403 and its relative absence in BPA-H. The formation of an alcohol functional group is a by-product of the curing reaction between an amine functional group and an epoxy ring, which is the case for the BPA/T-403 thermoset. However, for BPA-H, the alcohol functional groups were the reactive component that reacted with the epoxy ring, resulting in a decrease of alcohol functional groups and an increase in ether functional groups. The FTIR spectra shows no new carbonyl functional groups were formed after thermal treatment of both thermosets confirming that no thermal degradation is occurring at this exposure temperature and time.[38]

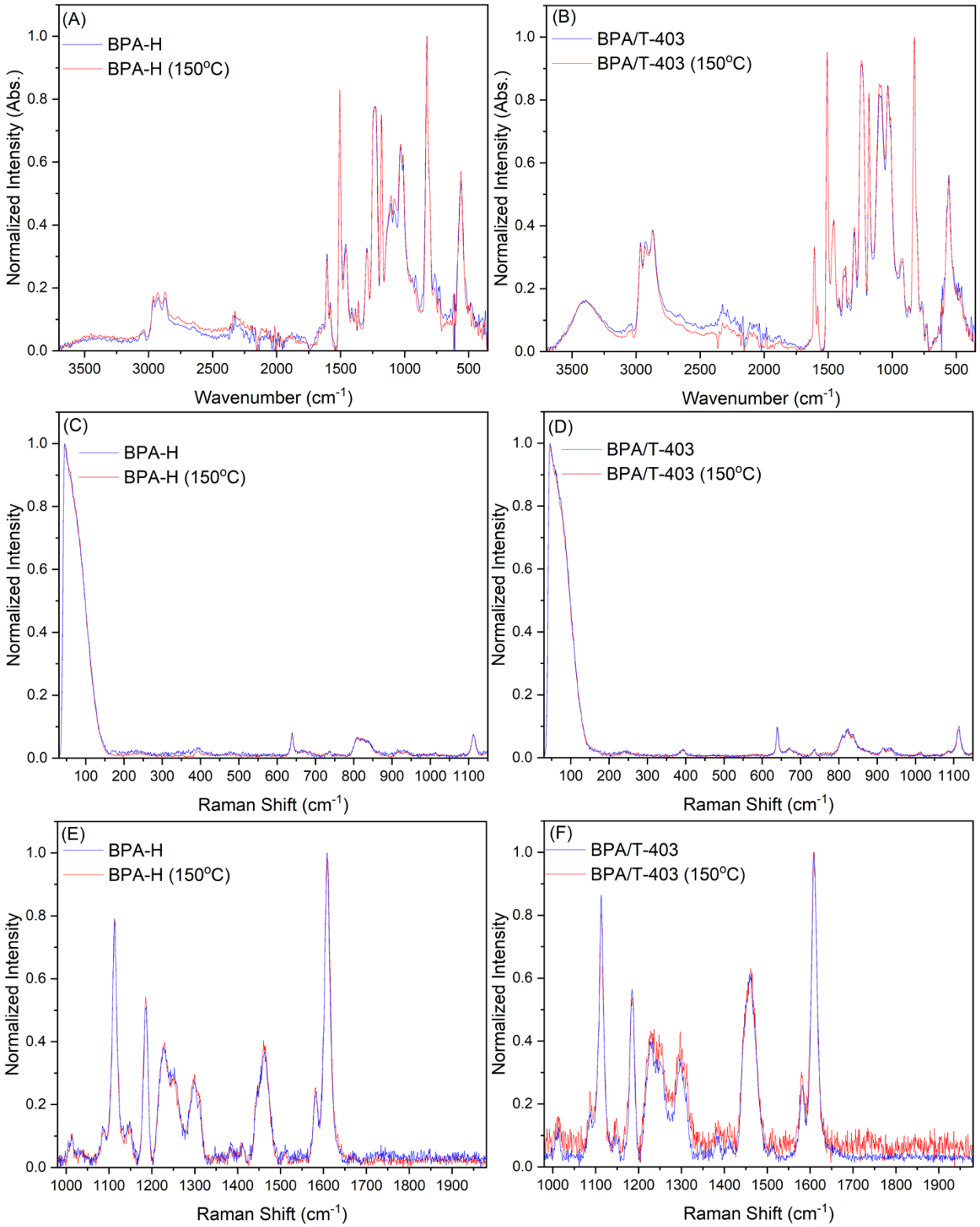

Figure 6. (A and B) FTIR and (C–F) Raman spectra of BPA-H and BPA/T-403 before and after thermal heating at 150 °C. Raman spectra were taken at two spectral ranges with (C and D) a low

range of 0–1200 cm^{-1} and (E and F) a high range of 900–2000 cm^{-1}. No change in chemical functionality was observed after thermal treatments, supporting the theory that no thermal degradation occurred.

PCA was used in this work to identify differences in the spectra of thermally treated and untreated thermosets. Numerous papers and books discuss in depth the details and application of PCA.[39-41] In short, PCA is a multivariate statistical technique that is used to extract important information from a data set and convert this information into a new set of orthogonal variables known as *principal components* (PCs). This conversion to variables reduces the data set's size into an abridged version of the original data, allowing for the identification of important variables. When developing a PCA model, a scree plot is routinely used to determine the number of components in the model. This plot is formed by plotting the calculated eigenvalues with respect to their size. The selection of the number of components from a scree plot is typically done by identifying the elbow or point at which the slope in the plot goes from steep to flat.[39]

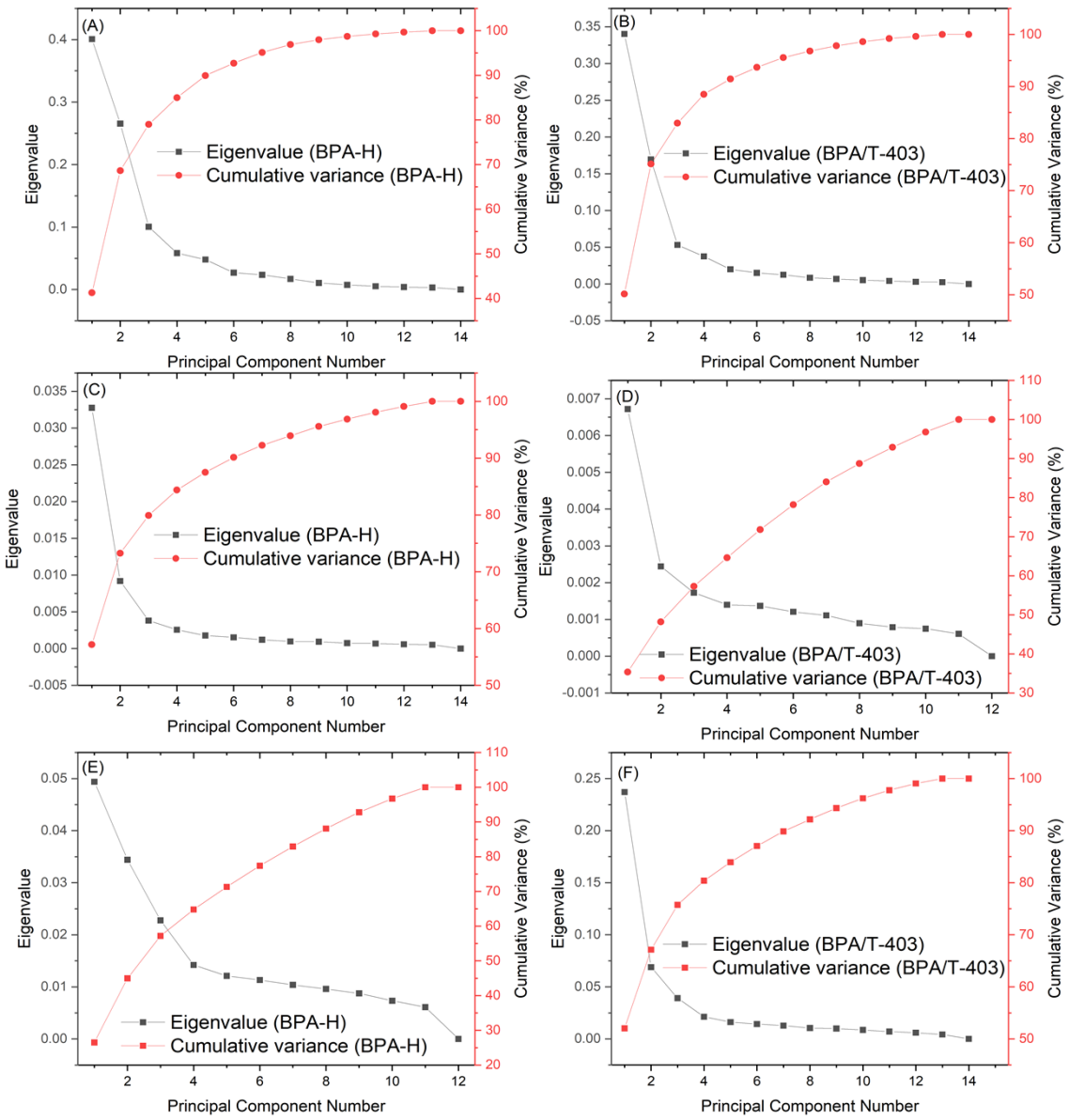

Figure 7. Scree plots from (A and B) PCA of FTIR spectra with PCA of Raman spectra for (C and D) low and (E and F) high Raman shift regions of BPA-H and BPA/T-403 before and after thermal heating at 150 °C.

Scree plots from PCA models of the FTIR and Raman data for both thermosets are shown in **Figure 7**. Three PCs were selected for the PCA models of the FTIR spectra, with cumulative variances summing to 79% for BPA-H and 83% for BPA/T-403, which show a good description of the data in **Figures 7A** and **7B**. Models for the Raman spectra were produced at two spectral

ranges using a low spectral range (0–1200 cm^{-1}) (**Figures 7C** and **7D**) and high spectral range (900–2000 cm^{-1}) (**Figures 7E** and **7F**). Three PCs for the low spectral range models were determined to be necessary and had cumulative variances summing to 80% for BPA-H and 57% for BPA/T-403 (**Figures 7C** and **7D**). Finally, for the high spectral range Raman models, four PCs were used for BPA-H spectra with a cumulative variance of 65%, and three PCs were used for BPA/T-403 with a cumulative variance of 76% (**Figures 7E** and **7F**).

With the number of PCs identified for each model, scores plots were made by plotting the resulting PCs against each other. Clustering in scores plots is indicative of measurable differences in the two data sets evaluated for each model. Scores plots for the FTIR models found the best clustering and separation between the pristine and thermally treated thermosets in plots PC1/PC2 and PC2/PC3 for BPA-H thermoset and PC2/PC3 for BPA/T-403 thermoset (**Figure 8)**. The remaining FTIR data score plots of PC1/PC3 for BPA-H and PC1/PC2 and PC1/PC3 for BPA/T-403 showed poor separation between the two sample types (see **Figure S1** in supplementary information). Raman spectra for the low Raman shift region of BPA-H and BPA-H treated at 150 °C had good separation for PC1/PC2 but poor separation for the remaining plots (**Figure S2**). The high Raman shift region for the BPA-H thermoset showed good separation for PC1/PC2, PC1/PC3, and PC1/PC4, but the remaining score plots had poor separation (**Figure S3**). Models produced from the low and high Raman shift regions of the BPA/T-403 thermoset showed no separation (**Figure S4**). Overall, the FTIR data had the most significant spectral alterations from thermal exposure based on the PCA models.

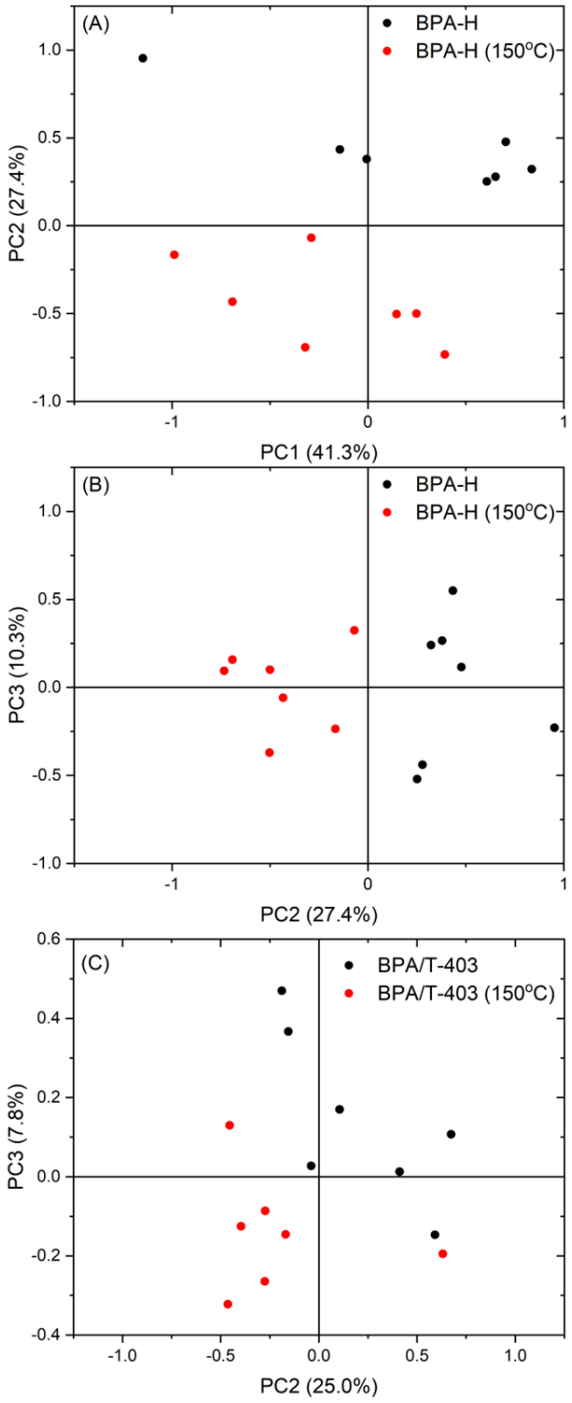

Figure 8. Score plots of FTIR spectra for (A) PC1/PC2 and (B) PC2/PC3 from BPA-H thermoset and (C) PC2/PC3 from BPA/T-403 thermoset. Clustering is observed between treated and untreated thermosets, indicating changes in the FTIR spectra after thermal heating.

The relationship between a specific component and a measured variable gives an estimate of the information that is shared between them. This relationship is called *loading*.[39] Loading plots of the selected score plots from FTIR can be used to identify the specific frequencies responsible for the observed separations in PCA. Loading plots of PC1 and PC2 for BPA-H (FTIR) show the most significant contributors to the variance in the PC1 component, which is from the signals associated with aromatic frequencies from 1400 to 1700 cm^{-1} (see **Figure 9A**). The ether and aromatics frequencies from 1000 to 1300 cm^{-1} are significant contributors for the PC2 component (**Figure 9C**).[38, 42, 43] PC3 from the BPA-H model shared similar contributions to that of PC1 (**Figure S5**). Close inspection of the aromatic frequencies from the PC1 plot (**Figure 9B**) shows an apparent decrease in signal intensity for the peaks identified with the loadings plot after thermal treatment. However, ether frequencies identified in PC2 show an increase in signal intensity (**Figure 9D**). The FTIR spectra of BPA-H also indicates that some additional curing occurred from a decrease in the observed epoxy peak at 915 cm^{-1} and is a factor in the PCA model for PC1 and PC2. Signals from 400 to 800 cm^{-1} also affect the model in both PCs, but their source is not known.

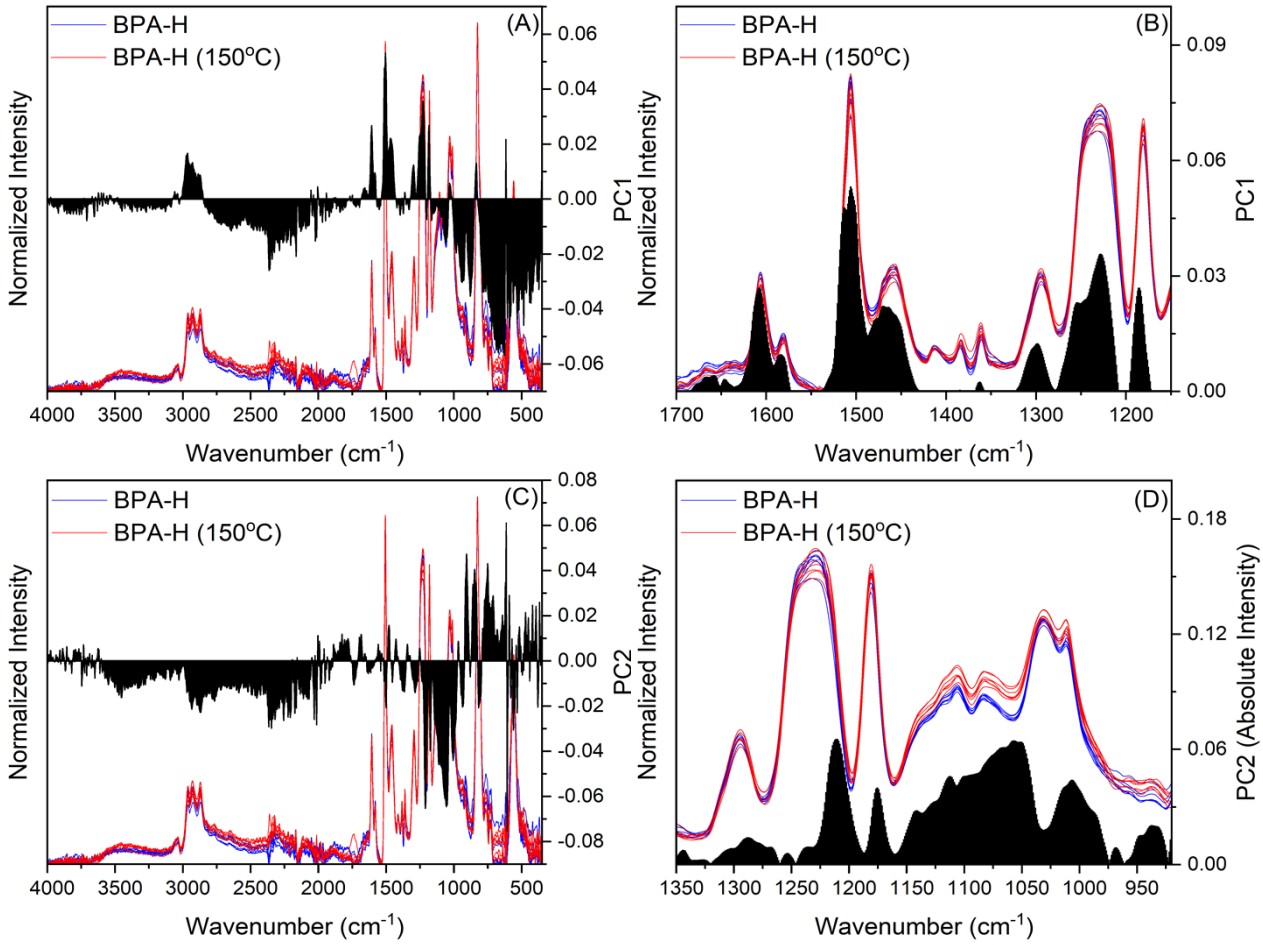

Figure 9. Loading plots of (A) PC1 and (C) PC2 overlaid onto BPA-H and BPA-H treated at 150 °C FTIR spectra with enlarged images of the most influential regions on observed separation in the model for (B) PC1 and (D) PC2, which are the aromatic and ether frequencies.

Loading plots from Raman models of BPA-H thermosets drew a similar conclusion as the FTIR models, but the differences were not as significant (**Figures S6–S9**). The loading plots of PC2 and PC3 (FTIR) for the BPA/T-403 thermoset does not show a strong influence from aromatic or ether frequencies on the PCA model (**Figures 10A** and **10C**), unlike the BPA-H models. The most defining and identifiable peak was observed in PC3 from 2800 to 3000 cm^{-1}. This range is associated with alkane frequencies. Some measurable changes from 900 to 1000 cm^{-1} were also observed and could be from additional curing in the thermoset, similar to that of BPA-H. The

influence of the alkane frequencies on PC3 appears to stem from a decrease in the center alkane peak after heating (**Figure 10B**). No discernable changes were observed in the FTIR ether frequencies that correlate to those in PC2 (**Figure 10D**). Considering that the most significant difference in the PCA models for the BPA/T-403 thermoset is from the alkane frequencies at 2800–3000 cm^{-1}, no significant differences were expected to be observed in the Raman models because these spectral frequencies were not measured in the two Raman measurements. The largest source of alkane functional groups is from the T-403 hardener; therefore, the spectral changes in the alkane frequencies and the change in C–C structure suggests that there was a rearrangement of the polymeric components of the hardener during heating.

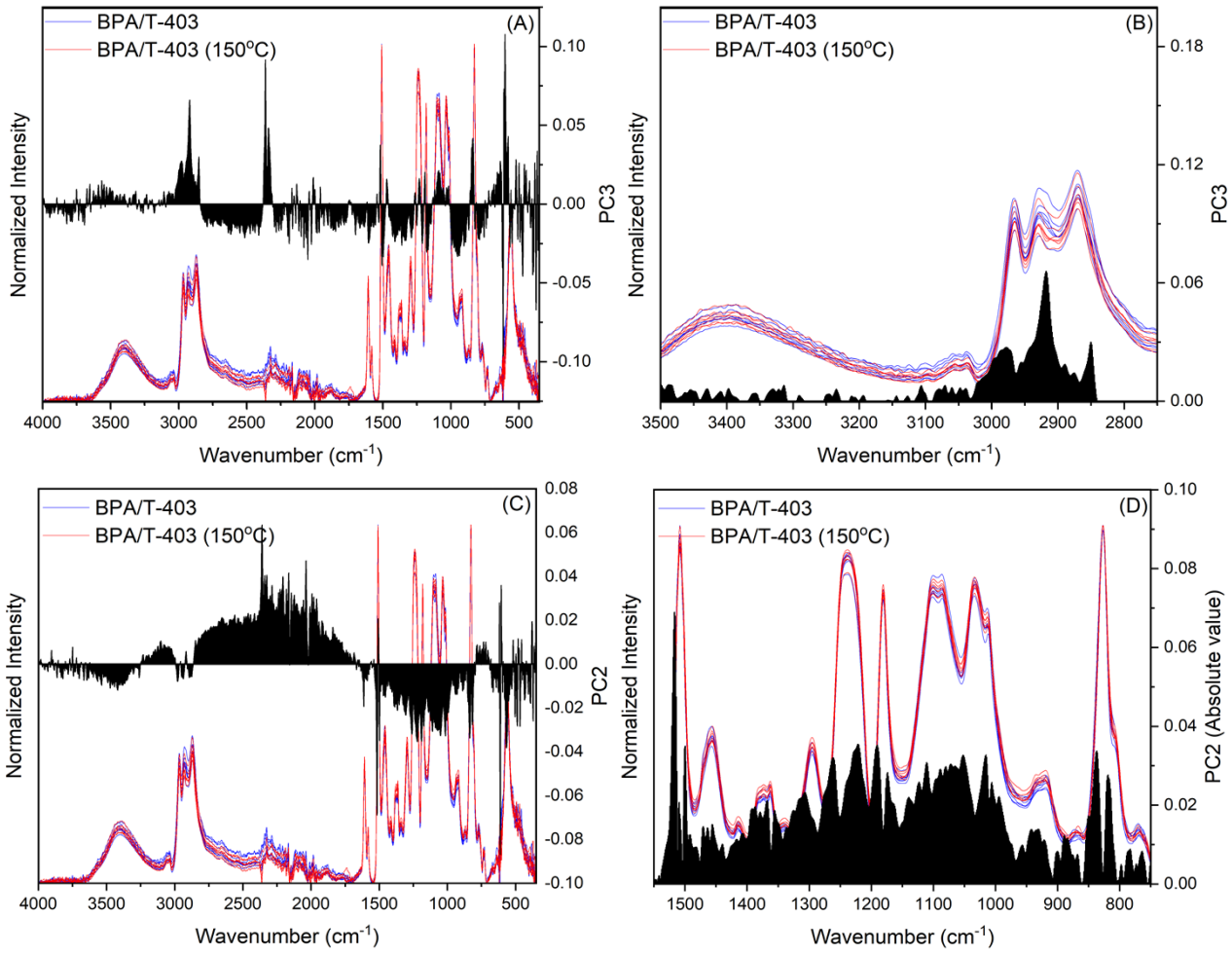

Figure 10. Loading plots of (A) PC3 and (C) PC2 overlaid onto BPA/T-403 and BPA/T-403 treated at 150 °C FTIR spectra with enlarged images of the most influential regions on observed separation in the model for (B) PC3 and (D) PC2, which are frequencies associated with alkanes.

The structural transitions of the hardener-to-hardener distance appeared to have the most significant influence on the spectroscopic response of the thermosets. The presence of changes in the hardener-to-hardener distance in BPA-H and absence in BPA/T-403 indicates that the homopolymerized system has a more rigid polymer network structure that does not pack efficiently at the set cure temperature of 85 °C. Heating allows for increased mobility of the polymer network and better rearrangement of the hardener groups for more efficient packing.

Another contributing factor to the significant alterations in the hardener-to-hardener distances in BPA-H could be further curing. Further curing would result in higher crosslinking density and potentially a decrease the hardener-to-hardener distance. However, the observed epoxy peak in FTIR before heating is small, indicating a high degree of cure before heating. The curing extent can be calculated by equation 1 and utilizing the stable aromatic peak at 1607 cm^{-1} compared to the epoxy ring peak at 914 cm^{-1} as it progresses through the curing process.[34, 44] Based on these calculations it was determined that the BPA-H thermoset is cured at approximately 81% and increases by 12 % after heating to 93%, **Figure 11**.

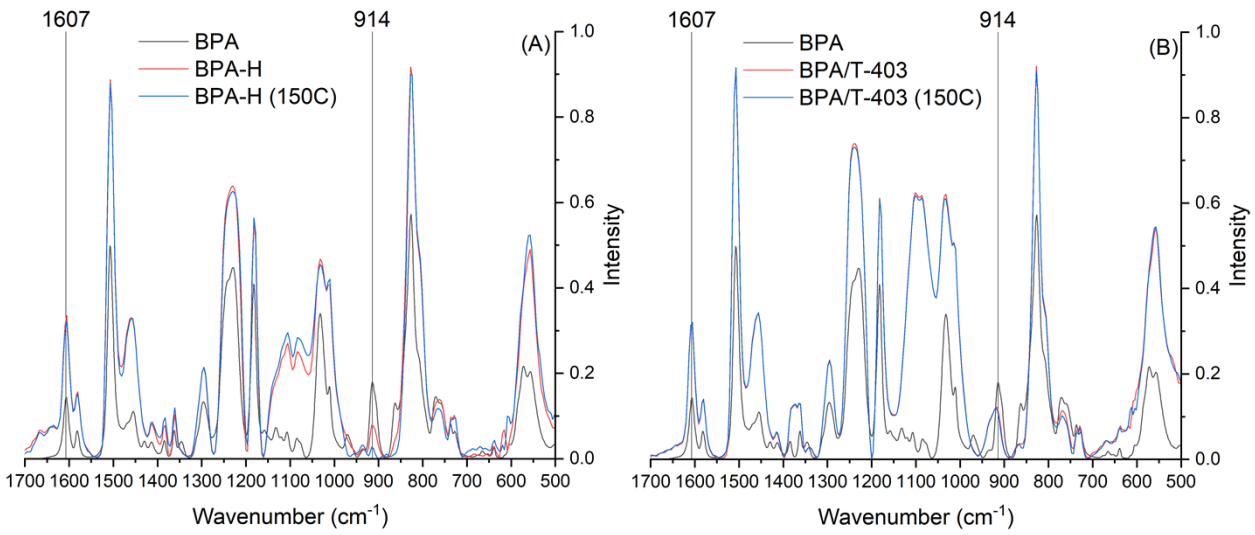

Figure 11. Averaged and normalized FTIR spectra of BPA-H (A) and BPA/T-403 (B) thermosets before and after heating at 150°C for 1hr with overlayed FTIR spectrum of BPA epoxy resin with stable aromatic stretch at 1607 cm^{-1} and epoxide ring stretch at 914 cm^{-1} marked.

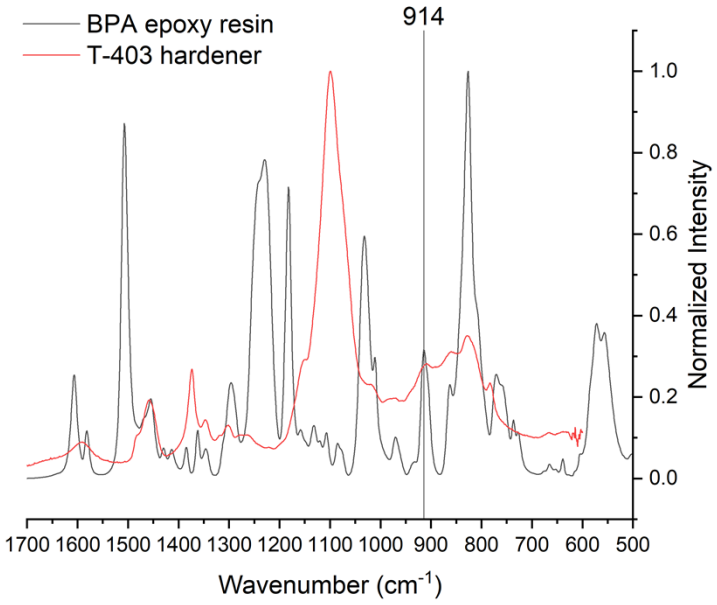

Figure 12. FTIR spectra of BPA epoxy resin and T-403 hardener showing signal overlap of T-403 hardener with epoxide frequency at 914 cm^{-1}.

Unfortunately, the same evaluation is difficult for BPA/T-403 due to signal overlap with the T-403 hardener at the epoxy peak, **Figure 12**. Nevertheless, we calculate 69% cure prior to heating

and no notable change after heating, but again this is likely due to the signal overlap of the hardener T-403 with the epoxy ring. It is unknown if minor increases in crosslinking density can result in the significant change seen in the average hardener-to-hardener distance in the polymer network but is unlikely as it would require additional crosslinking at each hardener-hardener site in the network to cause the observed complete shift in the H-H peak. In addition, the H-H peak intensity decreases after heating suggesting loss of this structure likely due to reorganization of the network. Further curing would increase the observed structure due to new structure formation suggesting the observed change is not entirely due to curing but from some other structural rearrangement.

Additionally, further curing in the BPA/T-403 thermoset is also likely, as indicated by PCA showing changes in the epoxy functional group region, but no changes in the hardener-to-hardener structure were observed. The intensity of the H–H structure in BPA/T-403 increased after thermal treatment, suggesting the additional formation of new H–H structures, which also supports additional curing. Because curing is evident in both thermosets but only significant changes in H-H are seen in BPA-H, this work proposes that the major observed shift in the BPA-H hardener-to-hardener distance is not solely because of additional curing but from rearrangement in the polymer network.

CONCLUSION

Using density functional theory, the structural origins of peaks observed in the WAXS of two epoxy thermosets have been identified as the hardener-to-hardener distance, aromatic π–π stacking, and the average Carbon–Carbon distances in the polymer system. Moderate thermal exposure of these thermosets at 150 °C was found to permanently alter these measured distances because of structural rearrangement in the polymer network. Using FTIR and Raman spectroscopy coupled with PCA, spectroscopic responses from structural rearrangement within the polymer

networks were observed. Although the direct source of change in the hardener-to-hardener distance is uncertain, this change elicits the largest response in the FTIR and Raman spectra with alterations in the aromatic and ether frequencies. This work lays the foundation for future investigations into the effects of structural alterations in thermoset polymer networks on measured material properties and demonstrates the ability to detect these structural alterations indirectly using FTIR and Raman spectroscopy.

AUTHOR INFORMATION

Corresponding Author

*dwyerdb@ornl.gov, Oak Ridge National Laboratory

ACKNOWLEDGMENTS

WAXS data measurements were carried out on a Xeuss 3 small-angle x-ray scattering/WAXS instrument via the Oak Ridge National Laboratory instrumentation pool. Resources and data interpretation were made possible via a full user proposal (proposal number: CNMS2022-A-01189) to the Center for Nanophase Materials Sciences, which is a US Department of Energy Office of Science User Facility.

ABBREVIATIONS

BPA, bisphenol A; BPA-H, homopolymerized bisphenol A; DSC, differential scanning calorimetry; FTIR, Fourier transform infrared spectroscopy; PC, principal component; PCA, principal component analysis; WAXS, wide-angle x-ray scattering.

ASSOCIATED CONTENT

Supporting Information. Score plots and loading plots of BPA-H and BPA/T-403 thermosets from FTIR and Raman spectra.

REFERENCES

1. Jin, F. L.; Li, X.; Park, S. J., Synthesis and application of epoxy resins: A review. *J. Ind. Eng. Chem.* **2015,** *29*, 1-11.
2. Montazeri, S.; Ranjbar, Z.; Rastegar, S.; Deflorian, F., A new approach to estimates the adhesion durability of an epoxy coating through wet and dry cycles using creep-recovery modeling. *Prog. Org. Coat.* **2021,** *159*, 106442.
3. Yeon, J., Deformability of Bisphenol A-Type Epoxy Resin-Based Polymer Concrete with Different Hardeners and Fillers. *Applied Sciences-Basel* **2020,** *10* (4), 1336.
4. Ozgul, E. O.; Ozkul, M. H., Effects of epoxy, hardener, and diluent types on the hardened state properties of epoxy mortars. *Construction and Building Materials* **2018,** *187*, 360-370.
5. dAlmeida, J. R. M.; Monteiro, S. N., The effect of the resin/hardener ratio on the compressive behavior of an epoxy system. *Polymer Testing* **1996,** *15* (4), 329-339.
6. Jang, C. W.; Kang, J. H.; Palmieri, F. L.; Hudson, T. B.; Brandenburg, C. J.; Lawson, J. W., Molecular Dynamic Investigation of the Structural and Mechanical Properties of Off-Stoichiometric Epoxy Resins. *ACS Appl. Polym. Mater.* **2021,** *3* (6), 2950-2959.
7. Minty, R. F.; Yang, L.; Thomason, J. L., The influence of hardener-to-epoxy ratio on the interfacial strength in glass fibre reinforced epoxy composites. *Composites Part a-Applied Science and Manufacturing* **2018,** *112*, 64-70.
8. Knox, S. T.; Wright, A.; Cameron, C.; Fairclough, J. P. A., Well-Defined Networks from DGEBF-The Importance of Regioisomerism in Epoxy Resin Networks. *Macromolecules* **2019,** *52* (18), 6861-6867.
9. Lv, G. X.; Jensen, E.; Shen, C. T.; Yang, K. X.; Evans, C. M.; Cahill, D. G., Effect of Amine Hardener Molecular Structure on the Thermal Conductivity of Epoxy Resins. *ACS Appl. Polym. Mater.* **2021,** *3* (1), 259-267.
10. Morgan, R. J.; Oneal, J. E., EFFECT OF EPOXY MONOMER CRYSTALLIZATION AND CURE CONDITIONS ON PHYSICAL STRUCTURE, FRACTURE TOPOGRAPHY, AND MECHANICAL RESPONSE OF POLYAMIDE-CURED BISPHENOL-A-DIGLYCIDYL ETHER EPOXIES. *J. Macromol. Sci.-Phys.* **1978,** *B15* (1), 139-169.
11. Schubach, H. R.; Nagy, E.; Heise, B., SHORT-RANGE ORDER OF AMORPHOUS POLYMERS DERIVED BY WAXS. *Colloid and Polymer Science* **1981,** *259* (8), 789-796.
12. Rabiej, S.; Wlochowicz, A., SAXS AND WAXS INVESTIGATIONS OF THE CRYSTALLINITY IN POLYMERS. *Angewandte Makromolekulare Chemie* **1990,** *175*, 81-97.
13. Heeley, E. L.; Gough, T.; Bras, W.; Gleeson, A. J.; Coates, P. D.; Ryan, A. J., Polymer processing: Using synchrotron radiation to follow structure development in commercial and novel polymer materials. *Nuclear Instruments & Methods in Physics Research Section B-Beam Interactions with Materials and Atoms* **2005,** *238* (1-4), 21-27.
14. Chuang, W. T.; Jeng, U. S.; Sheu, H. S.; Hong, P. D., Competition between phase separation and crystallization in a PCL/PEG polymer blend captured by synchronized SAXS, WAXS, and DSC. *Macromolecular Research* **2006,** *14* (1), 45-51.
15. Terrill, N. J.; Fairclough, P. A.; Towns-Andrews, E.; Komanschek, B. U.; Young, R. J.; Ryan, A. J., Density fluctuations: the nucleation event in isotactic polypropylene crystallization. *Polymer* **1998,** *39* (11), 2381-2385.

16. Gregorsvetec, D.; Malejkveder, S.; Zipper, P.; Janosi, A., WAXS STRUCTURAL-ANALYSIS OF POLYPROPYLENE FIBERS SPUN FROM 2 DIFFERENT POLYMER GRADES. *Chemical and Biochemical Engineering Quarterly* **1995,** *9* (3), 141-143.
17. Mossety-Leszczak, B.; Wlodarska, M.; Galina, H.; Bak, G. W.; Pakula, T., Development of liquid crystalline order during cure of mesogenic epoxy resins. *Macromolecular Symposia* **2005,** *227*, 149-160.
18. Grebowicz, J. S., On the formation of liquid crystalline texture in epoxy resins. *Macromolecular Symposia* **1996,** *104*, 191-221.
19. Cascaval, C. N.; Mititelu, A., Advanced materials based on epoxy resins - 3. Liquid crystalline polymers with biphenyl mesogen. *Materiale Plastice* **2005,** *42* (2), 120-123.
20. Mossety-Leszczak, B.; Galina, H.; Wlodarska, M.; Bak, G. W., Liquid crystal epoxies with biphenyl as a mesogenic group. *Przemysl Chemiczny* **2006,** *85* (8-9), 956-958.
21. Nigam, V.; Setua, D. K.; Mathur, G. N., Wide-angle X-ray scattering, Fourier transform infrared spectroscopy, and scanning electron microscopy studies on the influence of the addition of liquid functional rubber into epoxy thermoset. *J. Appl. Polym. Sci.* **1998,** *70* (3), 537-543.
22. Challis, R. E.; Freemantle, R. J.; Fuller, W.; Martin, C. M.; Mahendrasingham, A.; Chadwick, D.; Cocker, R. P., *Epoxy Cure Observed by Ultrasound, NMR and WAXS. In Thompson, D.O., Chimenti, D.E. (eds) Review of Progress in Quantitative Nondestructive Evaluation. Review of Progress in Quantitative Nondestructive Evaluation*. Springer, Boston, MA., 1999; Vol. 18A.
23. Lovell, R.; Windle, A. H., WAXS INVESTIGATION OF LOCAL-STRUCTURE IN EPOXY NETWORKS. *Polymer* **1990,** *31* (4), 593-601.
24. Hansen, J. P.; McDonald, I. R., *Theory of simple liquids*. 4th ed.; Academic Press: 2013.
25. Bras, W.; Derbyshire, G. E.; Devine, A.; Clark, S. M.; Cooke, J.; Komanschek, B. E.; Ryan, A. J., The Combination of Thermal-Analysis and Time-Resolved X-Ray Techniques - a Powerful Method for Materials Characterization. *Journal of Applied Crystallography* **1995,** *28*, 26-32.
26. Apra, E.; Bylaska, E. J.; de Jong, W. A.; Govind, N.; Kowalski, K.; Straatsma, T. P.; Valiev, M.; van Dam, H. J. J.; Alexeev, Y.; Anchell, J.; Anisimov, V.; Aquino, F. W.; Atta-Fynn, R.; Autschbach, J.; Bauman, N. P.; Becca, J. C.; Bernholdt, D. E.; Bhaskaran-Nair, K.; Bogatko, S.; Borowski, P.; Boschen, J.; Brabec, J.; Bruner, A.; Cauet, E.; Chen, Y.; Chuev, G. N.; Cramer, C. J.; Daily, J.; Deegan, M. J. O.; Dunning, T. H.; Dupuis, M.; Dyall, K. G.; Fann, G. I.; Fischer, S. A.; Fonari, A.; Fruchtl, H.; Gagliardi, L.; Garza, J.; Gawande, N.; Ghosh, S.; Glaesemann, K.; Gotz, A. W.; Hammond, J.; Helms, V.; Hermes, E. D.; Hirao, K.; Hirata, S.; Jacquelin, M.; Jensen, L.; Johnson, B. G.; Jonsson, H.; Kendall, R. A.; Klemm, M.; Kobayashi, R.; Konkov, V.; Krishnamoorthy, S.; Krishnan, M.; Lin, Z.; Lins, R. D.; Littlefield, R. J.; Logsdail, A. J.; Lopata, K.; Ma, W.; Marenich, A. V.; del Campo, J. M.; Mejia-Rodriguez, D.; Moore, J. E.; Mullin, J. M.; Nakajima, T.; Nascimento, D. R.; Nichols, J. A.; Nichols, P. J.; Nieplocha, J.; Otero-de-la-Roza, A.; Palmer, B.; Panyala, A.; Pirojsirikul, T.; Peng, B.; Peverati, R.; Pittner, J.; Pollack, L.; Richard, R. M.; Sadayappan, P.; Schatz, G. C.; Shelton, W. A.; Silverstein, D. W.; Smith, D. M. A.; Soares, T. A.; Song, D.; Swart, M.; Taylor, H. L.; Thomas, G. S.; Tipparaju, V.; Truhlar, D. G.; Tsemekhman, K.; Van Voorhis, T.; Vazquez-Mayagoitia, A.; Verma, P.; Villa, O.; Vishnu, A.; Vogiatzis, K. D.; Wang, D.; Weare, J. H.; Williamson, M. J.; Windus, T. L.; Wolinski, K.; Wong, A. T.; Wu, Q.; Yang, C.; Yu, Q.; Zacharias, M.; Zhang, Z.; Zhao, Y.; Harrison, R. J., NWChem: Past, present, and future. *Journal of Chemical Physics* **2020,** *152* (18).
27. Zhao, Y.; Truhlar, D. G., A new local density functional for main-group thermochemistry, transition metal bonding, thermochemical kinetics, and noncovalent interactions. *Journal of Chemical Physics* **2006,** *125* (19).
28. Grimme, S.; Antony, J.; Ehrlich, S.; Krieg, H., A consistent and accurate ab initio parametrization of density functional dispersion correction (DFT-D) for the 94 elements H-Pu. *Journal of Chemical Physics* **2010,** *132* (15).

29. Dunning, T. H., GAUSSIAN-BASIS SETS FOR USE IN CORRELATED MOLECULAR CALCULATIONS .1. THE ATOMS BORON THROUGH NEON AND HYDROGEN. *Journal of Chemical Physics* **1989,** *90* (2), 1007-1023.
30. Peterson, K. A.; Woon, D. E.; Dunning, T. H., BENCHMARK CALCULATIONS WITH CORRELATED MOLECULAR WAVE-FUNCTIONS .4. THE CLASSICAL BARRIER HEIGHT OF THE H+H-2- H-2+H REACTION. *Journal of Chemical Physics* **1994,** *100* (10), 7410-7415.
31. Wilson, A. K.; vanMourik, T.; Dunning, T. H., Gaussian basis sets for use in correlated molecular calculations .6. Sextuple zeta correlation consistent basis sets for boron through neon. *Theochem-Journal of Molecular Structure* **1996,** *388*, 339-349.
32. Woon, D. E.; Dunning, T. H., GAUSSIAN-BASIS SETS FOR USE IN CORRELATED MOLECULAR CALCULATIONS .3. THE ATOMS ALUMINUM THROUGH ARGON. *Journal of Chemical Physics* **1993,** *98* (2), 1358-1371.
33. Kendall, R. A.; Dunning, T. H.; Harrison, R. J., Electron affinities of the first-row atoms revisited. Systematic basis sets and wave functions. *The Journal of Chemical Physics* **1992,** *96*, 6796.
34. Fu, Y.; Sun, D. S.; Liu, X.; An, X. J.; Zhang, X. D., The curing kinetic analysis of epoxy based on FT-IR. *Proceedings of the 3rd International Conference on Material, Mechanical and Manufacturing Engineering* **2015,** *27*, 286-290.
35. Sinnokrot, M. O.; Valeev, E. F.; Sherrill, C. D., Estimates of the ab initio limit for pi-pi interactions: The benzene dimer. *J. Am. Chem. Soc.* **2002,** *124* (36), 10887-10893.
36. Dwyer, D. B.; Gallego, N. C.; Niedziela, J. L.; Kapsimalis, R. J.; Duckworth, D. C., Product Specific Thermal Degradation Kinetics of Bisphenol F Epoxy in Inert and Oxidative Atmospheres using Evolved Gas Analysis-Mass Spectrometry. *J. Anal. Appl. Pyrolysis* **2022,** *165*.
37. Dwyer, D. B.; Isbill, S. B.; Niedziela, J. L.; Kapsimalis, R. J.; Duckworth, D. C., Influence of temperature on accessible pyrolysis pathways of homopolymerized bisphenol A/F epoxies and copolymers. *J. Anal. Appl. Pyrolysis* **2021,** *153*.
38. Doblies, A.; Boll, B.; Fiedler, B., Prediction of Thermal Exposure and Mechanical Behavior of Epoxy Resin Using Artificial Neural Networks and Fourier Transform Infrared Spectroscopy. *Polymers* **2019,** *11* (2).
39. Abdi, H.; Williams, L. J., Principal Component Analysis. In *Wiley Interdisciplinary Reviews: Computational Statistics*, 2010; Vol. 2, pp 433-459.
40. Jolliffe, I.; Cadima, J., Principal component analysis: areview and recent developments. *Philosophical Transactions A* **2016,** *374*, 20150202.
41. Lever, J.; Krzywinski, M.; Naomi, A., Points of Significance Principal Component Analysis. *Nature Methods* **2017,** *14* (7), 641-642.
42. Nikolic, G.; Zlatkovic, S.; Cakic, M.; Cakic, S.; Lacnjevac, C.; Rajic, Z., Fast Fourier Transform IR Characterization of Epoxy GY Systems Crosslinked with Aliphatic and Cycloaliphatic EH Polyamine Adducts. *Sensors* **2010,** *10* (1), 684-696.
43. Cholake, S. T.; Mada, M. R.; Raman, R. K. S.; Bai, Y.; Zhao, X. L.; Rizkalla, S.; Bandyopadhyay, S., Quantitative Analysis of Curing Mechanisms of Epoxy Resin by Mid- and Near-Fourier Transform Infra Red Spectroscopy. *Defence Science Journal* **2014,** *64* (3), 314-321.
44. Theophanides, T., *Infrared Spectroscopy - Materials Science, Engineering and Technology*. InTech: 2012.

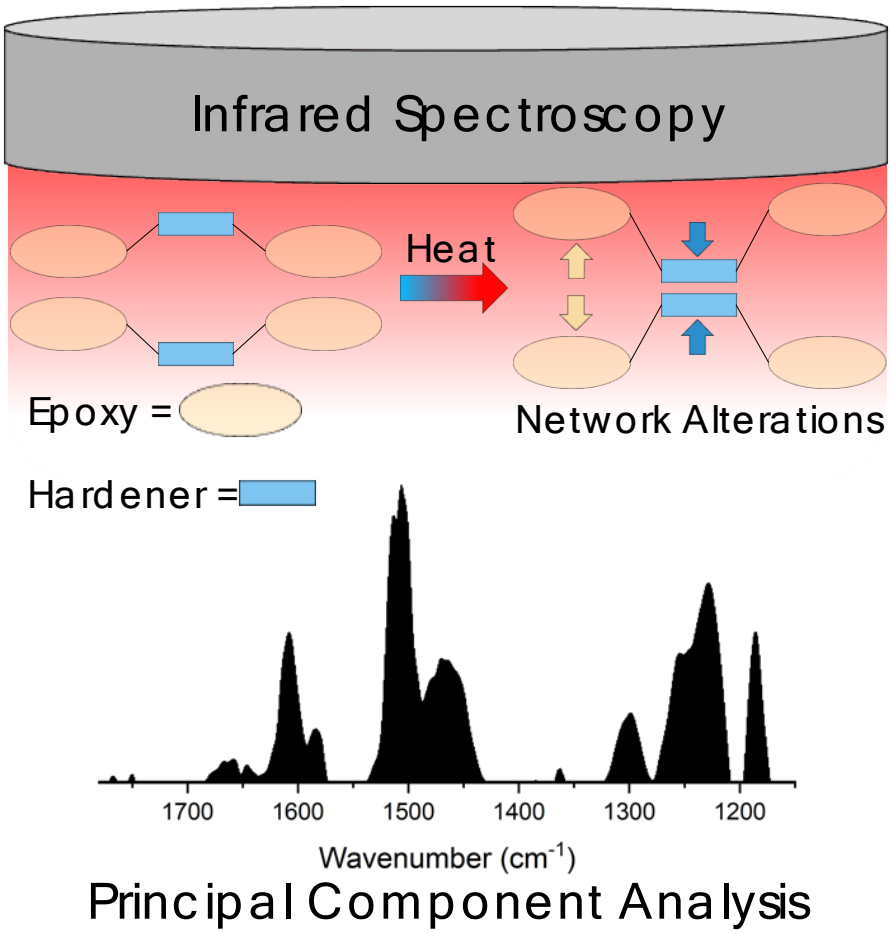

Table of content graphic